Dyes and Pigments 100 (2014) 127–134

Contents lists available at ScienceDirect

Dyes and Pigments

journal homepage: www.elsevier.com/locate/dyepig

Enhancing the coplanarity of the donor moiety in a donor-acceptor molecule to improve the efficiency of switching phenomenon for flash memory devices

Wusheng Ren, Hao Zhuang, Qing Bao, Shifeng Miao, Hua Li*, Jianmei Lu*, Lihua Wang

College of Chemistry, Chemical Engineering and Materials Science, China Petroleum and Chemical Industry Key Laboratory of Organic Wastewater Adsorption Treatment & Resource, Soochow University, Suzhou, Jiangsu 215123, China

ARTICLE INFO

Article history:
Received 2 July 2013
Received in revised form
28 August 2013
Accepted 2 September 2013
Available online 12 September 2013

Keywords:
Conjugated small molecules
Heck coupling
Coplanarity
Non-volatile
Flash memory
Surface morphology

ABSTRACT

Two conjugated small molecules were synthesized by Heck coupling reaction, wherein 1,8-naphthalimide acted as an electron acceptor, while either carbazole or triphenylamine, which contributed the different coplanarity, acted as electron donors, respectively. The devices based on both materials show non-volatile flash memory characteristics, and the effect of molecular coplanarity of the donor groups on the device performance was precisely studied. The results indicated that the reproducibility of the switching phenomenon for the memory device based on the carbazole containing naphthalimide derivative was much better than that based on the triphenylamino based naphthalimide due to the rigid carbazole moiety which improved the surface morphology as revealed by atomic force microscopy measurement. Therefore, the significance of the coplanarity of the donor moiety on improving reproducibility of switching phenomenon for memory device applications was revealed.

1. Introduction

Organic materials have been widely investigated for data storage devices due to scalability, structural flexibility, low cost, and three-dimensional stacking capability [1–8]. A large number of organic compounds, including conjugated polymers [9–15], oligomers [16,17], blends of nanoparticles [18–20] and small organic molecules [21–25], have been reported for electrical switching and memory devices. Especially, organic donor-acceptor (D–A) molecules, due to their ability to exhibit electrical bistability and versatility in molecular design, have received considerable attention [26–29]. Currently, many groups use donor (D) – acceptor (A) switching materials to meet the requirements of high-density data storage. However, the research had been mainly focused on the exploration of different D–A molecules with better electrical properties for data storage. The coplanarity of the terminal donor moiety which changes the surface morphology of the thin film formed by vacuum evaporation affecting the reproducibility of the switching phenomenon for the memory devices, had rarely been precisely studied. A better understanding of the effect of terminal moiety coplanarity on device performance is essential to help design new D–A molecules for memory devices.

Herein, we designed and synthesized two novel D–A molecules (NI-Cz and NI-TPA) with the same electron-accepting 1,8-naphthalimide (NI) moiety which was an attractive deficient electron moiety and had been widely utilized in both small molecule and polymer based memory devices [30,31]. Triphenylamine (TPA) derivatives have good optical properties and hole-transporting ability, but their morphology was amorphous with rougher surface due to the twisted triphenylamine moiety [32–35]. The carbazole (Cz) molecule, also a well-known electron-donor and hole-transporting group, and its substituted analogues have been widely used in the photovoltaic devices and memory devices due to its unique electronic and photochemical properties [36–39]. Compared to the triphenylamine derivatives, the surface morphology of carbazole derivatives was more coplanar due to the rigid carbazole moiety. The study showed that the coplanarity of the terminal group played a key role for the reproducibility of switching phenomenon of the memory devices. For the device based NI-Cz, the turn-on voltage was mainly between −2.2 V and −2.6 V (with yield of 80%), and turn-off voltage was mainly between 2.6 V and 3 V (with yield of 56%). For NI-TPA, the turn-on voltage varied from −0.4 V to −2.0 V, and the turn-off voltage was from 2.4 V to 4.0 V, and it showed no obvious distributed areas.

* Corresponding authors. Tel.: +86 512 65880368; fax: +86 512 65880367.
E-mail addresses: jianmeilu_group@hotmail.com (H. Li), lujm@suda.edu.cn (J. Lu).

0143-7208/$ – see front matter © 2013 Elsevier Ltd. All rights reserved.
http://dx.doi.org/10.1016/j.dyepig.2013.09.002

This work takes an important step towards rational design of new organic D–A molecules with suitable structures for better reproducibility of switching phenomenon for the memory devices.

2. Experimental

2.1. Materials

4-Bromo-1,8-naphthalic anhydride, 2-ethylhexan-1-amine, palladium diacetate, tri-*o*-tolylphosphine, methyltriphenylphosphonium bromide, potassium *tert*-butanolate, triphenylamine and carbazole were all purchased from Energy Chemical as analytical regents and used without further purification. N,N-Dimethylformamide (DMF) was dried by distillation over CaH_2. Other reagents were used as received without any further purification.

2.2. Instruments

All electrical measurements of the device were characterized under ambient conditions without any encapsulation using an HP 4145B semiconductor parameter analyzer equipped with an HP 8110A pulse generator. NMR spectra were obtained from an Inova 400 FT-NMR spectrometer. High-resolution mass spectra (HRMS) were determined on Micromass GCT-TOF mass spectrometer with an ESI source. Elemental analysis was performed using a Carlo-Erba EA-1110 instrument. UV–Vis absorption spectra were measured at room temperature by using a Shimadzu UV-3600 spectrophotometer. Cyclic voltammetry was performed at room temperature using an ITO working electrode, a reference electrode Ag/AgCl, and a counter electrode (Pt wire) at a sweep rate of 100 mV/s (CorrTest CS Electrochemical Workstation analyzer). A 0.1 M solution of tetrabutylammonium perchlorate (TBAP) in anhydrous DMF was used. SEM images were taken on a Hitachi S-4700 scanning electron microscope. Atomic force microscopy (AFM) measurements were performed by using an MFP-3DTM (Digital Instruments/Asylum Research) AFM instrument.

2.3. Synthesis of NI–Cz and NI–TPA

The two molecules were synthesized by Heck coupling reaction in good yields as shown in Scheme 1.

4-Bromo-N-(2-ethylhexyl)-1,8-naphthalimide (**1**). A solution of 4-bromo-1,8-naphtalic anhydride (5 g, 18.05 mmol) in ethanol (100 mL) was added to a 250 mL three-neck round bottom equipped with a reflux condenser and a magnetic stirrer. Then 2-ethylhexan-1-amine (2.33 g, 18.05 mmol) was added drop-wise and the reaction mixture was heated up to 110 °C and stirred under nitrogen overnight. The mixture was cooled to room temperature, and it was filtered. The filtrate was purified by silica gel column chromatography using a mixture of petroleum and dichloromethane (vol. ratio 5:1) as an eluent. After recystallization from the eluent mixture of solvents, yellow crystals were obtained with a yield of 95.01%. Mp = 82–83 °C. IR (in KBr), cm^{-1}: 3071, 2959, 2926, 2871, 2855, 1702, 1653, 1615, 1590, 1571, 1504, 1460,1435, 1404, 1344, 1278, 1231, 1182, 1150, 1102, 1083, 1044, 1024, 949, 897, 855, 782, 749, 730, 716, 664. ^{1}H NMR (400 MHz, $CDCl_3$) δ 8.65 (d, J = 7.3 Hz, 1H), 8.56 (d, J = 8.5 Hz, 1H), 8.41 (d, J = 7.8 Hz, 1H), 8.04 (d, J = 7.9 Hz, 1H), 7.85 (t, J = 7.9 Hz, 1H), 4.18–4.04 (m, 2H), 2.01–1.85 (m, 1H), 1.43–1.27 (m, 8H), 0.93 (t, J = 7.4 Hz, 3H), 0.87 (t, J = 6.8 Hz, 3H). Anal. Calcd. for $C_{20}H_{22}BrNO_2$: C, 61.86; H, 5.71; N, 3.61. Found: C, 61.82; H, 5.75; N, 3.57.

4-(9H-carbazol-9-yl)benzaldehyde (**2**). A mixture of 9H-Carbazole (5 g, 0.03 mol), and sodium hydroxide (1.2 g, 0.03 mol) in dry dimethylformamide (DMF) was heated with stirring. Then 4-fluorobenzaldehyde (3.72 g, 0.03 mol) was added, and the reaction mixture was stirred at 130 °C for 6 h. After cooling to room temperature, the mixture was poured into distilled water and extracted with ethyl acetate. The organic layer was dried with anhydrous magnesium sulfate and concentrated by vacuum evaporation. The crude product was purified by column chromatography using the mixture of petroleum and dichloromethane (vol. ratio 3:1) as an eluent to get the desired compound as a yellow solid (6.43 g) with a yield of 79.08%. Mp = 156–157 °C. IR (in KBr), cm^{-1}: 2733, 1910, 1702, 1597, 1566, 1510, 1478, 1451, 1389, 1361, 1336, 1316, 1300, 1226, 1208, 1181, 1161, 1123, 1103, 1023, 1000, 914, 829, 750, 720, 633, 619, 566. ^{1}H NMR (400 MHz, $CDCl_3$) δ 10.12 (s, 1H), 8.20–8.10 (m, 4H), 7.80 (d, J = 8.3 Hz, 2H), 7.51 (d, J = 8.2 Hz, 2H), 7.44 (t, J = 7.6 Hz, 2H), 7.34 (t, J = 7.4 Hz, 2H). Anal. Calcd. for $C_{19}H_{13}NO$: C, 84.11; H, 4.83; N, 5.16. Found: C, 84.07; H, 4.87; N, 5.15.

9-(4-Vinylphenyl)-9H-carbazole (**3**). A mixture of **2** (2.71 g, 10 mmol), potassium *tert*-butylate (1.68 g, 15 mmol), and CH_3PPh_3Br (4.28 g, 12 mmol) in dry THF (100 mL) under nitrogen was stirred for 24 h the mixture was poured into distilled water and

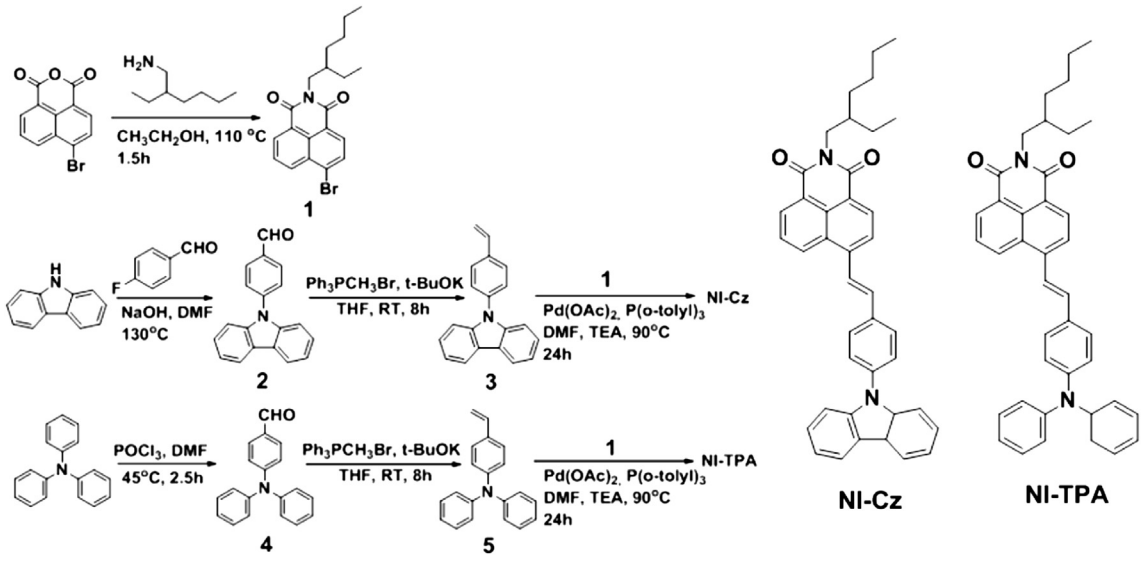

Scheme 1. Synthetic routes and molecular structures of NI–Cz and NI–TPA.

extracted with ethyl acetate. The organic layer was dried with anhydrous magnesium sulfate and concentrated by vacuum evaporation. The crude product was purified by column chromatography using the mixture of petroleum and dichloromethane (vol. ratio 5:1) as an eluent to get the desired compound as a white solid (2.43 g) with a yield of 90.34%. Mp = 117–118 °C. IR (in KBr), cm^{-1}: 1655, 1628, 1595, 1513, 1478, 1453, 1361, 1335, 1319, 1229, 1186, 1112, 1014, 985, 912, 838, 749, 724, 654, 618, 568. ^1H NMR (400 MHz, $CDCl_3$) δ 8.16 (d, J = 7.7 Hz, 2H), 7.65 (d, J = 8.3 Hz, 2H), 7.54 (d, J = 8.4 Hz, 2H), 7.47–7.40 (m, J = 0.9 Hz, 4H), 7.30 (d, J = 2.3 Hz, 2H), 6.84 (dd, J = 17.6, 10.9 Hz, 1H), 5.87 (d, J = 17.6 Hz, 1H), 5.38 (d, J = 10.9 Hz, 1H). Anal. Calcd. for $C_{20}H_{15}N$: C, 89.19; H, 5.61; N, 5.20. Found: C, 89.16; H, 5.64; N, 5.20.

4-(Diphenylamino)benzaldehyde (**4**). Phosphorus oxychloride (24 mL, 315 mmol) was added dropwise to DMF (30 mL) at 0 °C, and the mixture was stirred for 1 h at this temperature. Then triphenylamine (10 g, 40 mmol) was added, and the reaction mixture was stirred at 100 °C for 6 h. When the reaction was finished the mixture was cooled to room temperature, poured into ice water, and neutralized to pH 7 with 5% NaOH aqueous solution. The solution was extracted with ethyl acetate. The organic layer was dried with anhydrous magnesium sulfate and concentrated by vacuum evaporation. The crude product was purified by column chromatography using the mixture of petroleum and dichloromethane (vol. ratio 2:1) as an eluent to get the desired compound as a pale yellow solid (5.76 g) with a yield of 52.74%. Mp = 120–121 °C. IR (in KBr), cm^{-1}: 2741, 1688, 1584, 1503, 1488, 1450, 1427, 1330, 1304, 1288, 1269, 1219, 1185, 1155, 1111, 1074, 1028, 906, 824, 769, 757, 696, 616, 535. 1H NMR (400 MHz, $CDCl_3$) δ 9.81 (s, 1H), 7.68 (d, J = 8.6 Hz, 2H), 7.34 (t, J = 7.7 Hz, 4H), 7.17 (d, J = 6.9 Hz, 6H), 7.01 (d, J = 8.5 Hz, 2H). Anal. Calcd. for $C_{19}H_{15}NO$: C, 83.49; H, 5.53; N, 5.12. Found: C, 83.47; H, 5.57; N, 5.12.

4-Vinyltriphenylamine (**5**). 5 was prepared by the same procedure as compound 3 using 4 (2.73 g, 10 mmol), potassium *tert*-butylate (1.68 g, 15 mmol), and CH_3PPh_3Br (4.28 g, 12 mmol). The crude product was purified by column chromatography using the mixture of petroleum and dichloromethane (vol. ratio 5:1) as an eluent to get the desired compound as a white solid (2.23 g) with a yield of 82.28%. Mp = 90–91 °C. IR (in KBr), cm^{-1}: 1625, 1590, 1506, 1486, 1411, 1328, 1283, 1267, 1175, 1074, 1026, 990, 890, 839, 758, 699, 649, 616, 581, 512, 490. ^1H NMR (400 MHz, $CDCl_3$) δ 7.28 (d, J = 8.6 Hz, 2H), 7.23 (d, J = 8.0 Hz, 4H), 7.09 (d, J = 7.8 Hz, 4H), 7.02 (d, J = 8.0 Hz, 4H), 6.66 (dd, J = 17.6, 10.9 Hz, 1H), 5.63 (d, J = 17.6 Hz, 1H), 5.15 (d, J = 10.9 Hz, 1H). Anal. Calcd. for $C_{20}H_{17}N$: C, 88.52; H, 6.31; N, 5.16. Found: C, 88.50; H, 6.34; N, 5.16.

(E)-6-(4-(4aH-carbazol-9(9aH)-yl)styryl)-2-(2-ethylhexyl)-1,8-naphthalimide **(NI-Cz)**. A flask was charged with a mixture of 1 (0.50 g, 1.29 mmol), 3 (0.42 g, 1.55 mmol), $Pd(OAc)_2$ (5 mg, 0.016 mmol), P(*o*-tolyl)$_3$ (16 mg, 0.071 mmol), DMF (10 mL), and triethylamine (3 mL). The flask was degassed and purged with N_2. The mixture was heated at 90 °C for 24 h under N_2. Then, it was filtered, and the filtrate was poured into distilled water and extracted with ethyl acetate. The organic layer was dried with anhydrous magnesium sulfate and concentrated by vacuum evaporation. The crude product was purified by column chromatography using the mixture of petroleum and dichloromethane (vol. ratio 2:1) as an eluent to get the desired compound as a orange-yellow solid (0.46 g) with a yield of 61.33%. Mp = 210–211 °C. IR (in KBr), cm^{-1}: 3034, 2957, 2925, 1694, 1656, 1584, 1478, 1452, 1384, 1232, 1184, 1090, 964, 780, 752, 722. ^1H NMR (400 MHz, $CDCl_3$) δ 8.70–8.59 (m, 3H), 8.17 (d, J = 7.7 Hz, 2H), 8.07 (d, J = 7.7 Hz, 1H), 8.00 (d, J = 16.0 Hz, 1H), 7.89 (d, J = 8.3 Hz, 2H), 7.85–7.79 (m, 1H), 7.67 (d, J = 8.4 Hz, 2H), 7.53–7.40 (m, 5H), 7.32 (t, J = 7.3 Hz, 2H), 4.15 (qd, J = 12.8, 7.3 Hz, 2H), 1.96 (d, J = 6.8 Hz, 1H), 1.43–1.27 (m, 8H), 0.95 (t, J = 7.4 Hz, 3H), 0.89 (t, J = 7.0 Hz, 3H). Anal. Calcd. for $C_{40}H_{36}N_2O_2$: C, 83.30; H, 6.29; N, 4.86. Found: C, 83.25; H, 6.32; N, 4.84.

(E)-6-(4-(N,N-diphenyl)styryl)-2-(2-ethylhexyl)-1,8-naphthalimide (**NI–TPA**). NI-TPA was prepared by the same procedure as compound NI-Cz using 1 (0.50 g, 1.29 mmol), 5 (0.42 g, 1.55 mmol), $Pd(OAc)_2$ (5 mg, 0.016 mmol), P(*o*-tolyl)$_3$ (16 mg, 0.071 mmol), DMF (10 mL), and triethylamine (3 mL). The crude product was purified by column chromatography using the mixture of petroleum and dichloromethane (vol. ratio 2:1) as an eluent to get the desired compound as a red solid (0.39 g) with a yield of 52% [31]. Mp = 157–158 °C. IR (in KBr), cm^{-1}: 3034, 2955, 2926, 2857, 1698, 1656, 1585, 1508, 1491, 1439, 1385, 1350, 1282, 1233, 1178, 1092, 1026, 964, 846, 831, 782, 751, 695, 617, 526. ^1H NMR (400 MHz, $CDCl_3$) δ 8.63 (d, J = 7.2 Hz, 1H), 8.58 (d, J = 8.0 Hz, 2H), 7.98 (d, J = 7.8 Hz, 1H), 7.82 – 7.70 (m, 2H), 7.51 (d, J = 8.4 Hz, 2H), 7.34–7.27 (m, 5H), 7.15 (d, J = 7.8 Hz, 4H), 7.10 (d, J = 10.4 Hz, 4H), 4.21–4.05 (m, 2H), 1.96 (s, 1H), 1.40–1.27 (m, 8H), 0.94 (t, J = 7.3 Hz, 3H), 0.88 (t, J = 6.6 Hz, 3H). Anal. Calcd. for $C_{40}H_{38}N_2O_2$: C, 83.01; H, 6.62; N, 4.84. Found: C, 82.93; H, 6.71; N, 4.88.

2.4. Device fabrication and characterization

The electrical properties of the two D–A molecules were evaluated in Al/molecule/ITO sandwich structures. The ITO glass substrates were pre-cleaned in ultrasonic bath for 15 min each in detergent, de-ionized water, acetone, and alcohol. The substituted naphthalimide (25 mg) was deposited onto the pre-cleaned ITO substrates by vacuum evaporation. The resultant film thickness was around 70 nm which was measured by scanning electron microscope (SEM) as shown in the Fig. 1. Al top electrodes were deposited onto the film surface via thermal evaporation at 10^{-6} Torr through a shadow mask.

3. Results and discussion

3.1. Thermal gravimetric analysis of NI–Cz, NI–TPA

The thermal properties of NI–Cz and NI–TPA were investigated by TGA as shown in Fig. 2. Both compounds exhibit good thermal stability with thermal decomposition temperatures (5% weight loss temperature) of 323.86 °C (NI–Cz) and 407.06 °C (NI–TPA), respectively. It indicates that the materials can endure heat exposure in the memory devices.

3.2. Optical properties and electrochemical properties

The UV–vis absorption spectra of the two conjugated compounds in dilute DCM solution and in the thin films are shown in Fig. 3. In solution the high-energy absorption bands (294 nm, 307 nm and 342 nm) can be attributed to the π–π* transition of

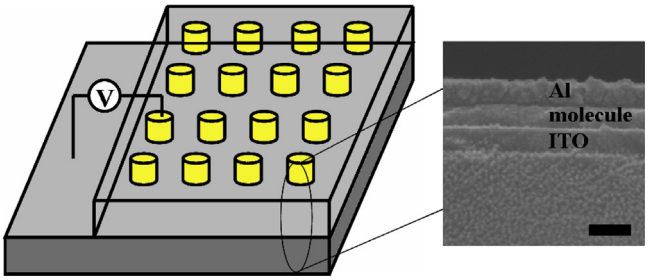

Fig. 1. Schematic diagram of the memory device with thin film of NI–Cz or NI–TPA sandwiched between an indium-tin-oxide (ITO) substrate and an aluminum top electrode. The scale bar is 100 nm.

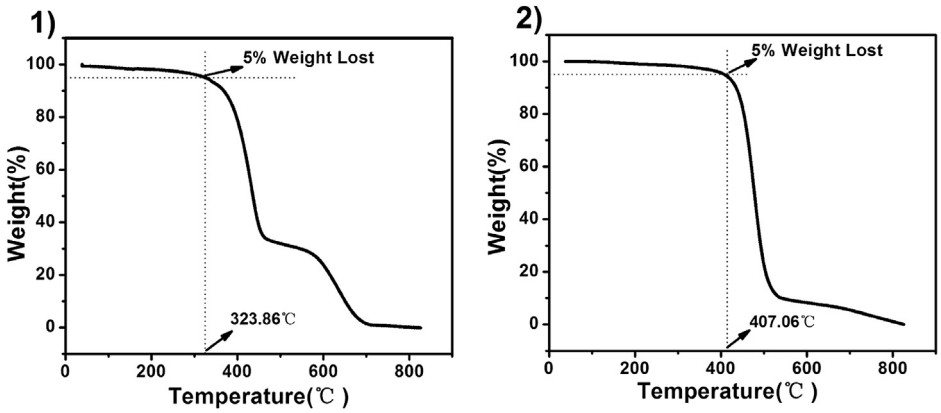

Fig. 2. TGA curves of NI–Cz (1), NI–TPA (2) measured in nitrogen atmosphere at a heating rate of 10 °C/min.

carbazole, triphenylamine and 1,8-naphthalimide moieties, and the low-energy absorption bands (403 nm and 457 nm) arise from the intramolecular charge transfer (ICT) [31]. Compared with the absorption spectra in solution state, the intramolecular charge transfer (ICT) transition absorption peaks in the solid film state are obviously red-shifted (NI–Cz from 403 to 416 nm, and NI–TPA from 457 to 467 nm) and significantly broadened. The red-shift and broadened absorption peaks from solution to solid state might be associated with the formation of molecular aggregation or orderly π–π stacking, so the absorption spectrum of the film of the NI–Cz molecule broadened more than NI–TPA due to its coplanar carbazole moiety that more readily participates in π–π stacking. In addition, the optical bandgaps (E_g^{opt}) of NI–Cz and NI–TPA films determined from the onset of optical absorbance can be estimated to be about 2.51 and 2.19 eV, respectively.

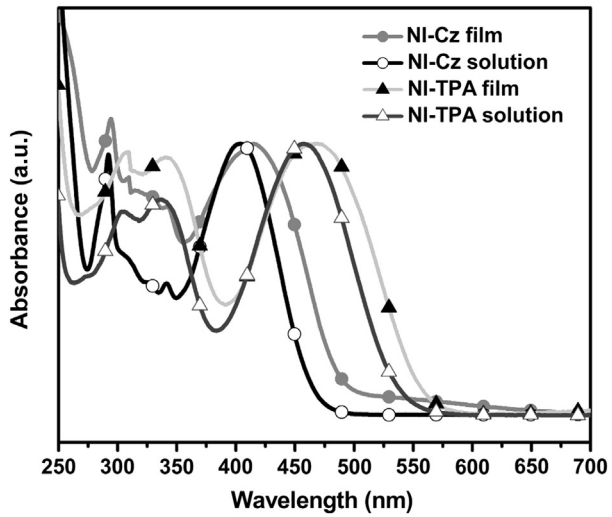

Fig. 3. UV–Vis absorption spectra of NI–Cz and NI–TPA in dilute DCM solution and solid thin film on quartz glass substrate.

Fig. 4 shows the cyclic voltammograms of the two molecules recorded in solution. Pertinent electrochemical data are summarized in Table 1. Both molecules exhibited one irreversible oxidation wave corresponding to the oxidation of the carbazole or triphenylamine donor moieties with the oxidation peaks at 1.42 and 0.98 eV for NI–Cz and NI–TPA, respectively. The HOMO energy levels can be calculated from the onset oxidation potential with reference to ferrocene (4.8 eV) by the following equation HOMO (eV) = –[E_{ox} (onset) *vs* Ag/AgCl + 4.8 – $E_{1/2}$ (ferrocene)], whereas the LUMO energy levels can be determined from the difference between the HOMO and the optical bandgap. The HOMO and LUMO values were determined to be −5.66 (or −5.22) and −3.15 (or −2.54) eV for the NI–Cz (or NI–TPA) film.

The HOMO and LUMO energy levels of the two molecules and the work function of Al top and ITO bottom electrodes were considered here to understand the memory behavior of the molecule based devices. For NI-Cz the energy barrier between ITO (–4.8 eV) and HOMO energy which was 0.86 eV which was lower than that between Al (–4.28 eV) and the LUMO energy level was 1.13 eV, this indicated that hole injection from ITO into the HOMO of NI–Cz was much easier than the electron injection from Al into LUMO of the compound. Thus, NI–Cz was a *p*-type material and holes controlled the conduction process. NI-TPA was also *p*-type material

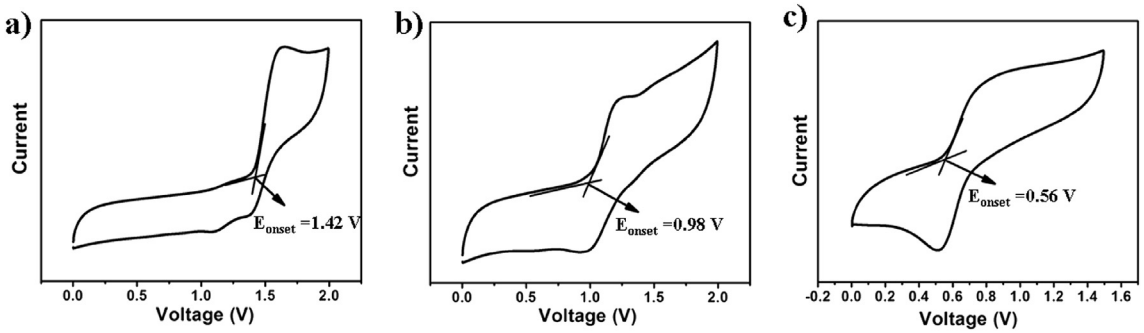

Fig. 4. Cyclic voltammograms of NI–Cz (a), NI–TPA (b) and Ferrocene (c) in anhydrous CH_2Cl_2 containing Bu_4NClO_4 (0.1 mol/L) with Ag/AgCl as reference electrode and Pt wire as counter electrode. A scan rate 100 mV/s was used.

Table 1
HOMO–LUMO energy levels, optical and electrochemical band-gap energies, and ionization potentials of NI–Cz and NI–TPA.

Molecule	E_{HOMO} (eV)[a]	E_{LUMO} (eV)[b]	E_g^{elc} (eV)[c]	E_g^{opt} (eV)[d]
NI-Cz	–5.66 (–5.50)[e]	–3.15 (–2.72)[e]	2.78	2.51
NI-TPA	–5.22 (–5.14)[e]	–3.03 (–2.54)[e]	2.6	2.19

[a] $E_{HOMO} = -(E_p + 4.8)$ (eV).
[b] $E_{LUMO} = -(E_n + 4.8)$ (eV) (where E_n and E_p are onset oxidation potentials versus the Fc/Fc+).
[c] Having HOMO and LUMO bands value, it is simple to calculate electrochemical band gap $Eg^{elc} = E_{LUMO} - E_{HOMO}$ (eV).
[d] The optical band gap estimated from the onset wavelength of optical absorption according to the formula $E_g = 1240/\lambda_{edge}$, in which the λ_{edge} is the onset value of absorption spectrum in long-wave direction.
[e] Corresponding to the model compounds NI-CZ, NI-TPA calculated at the B3LYP/6-31G level.

deduced from UV–vis absorption spectra and the CV measurements.

3.3. Morphology of the thin films

Atomic force microscopy (AFM) was used to characterize the surface morphology of the vacuum-deposited electroactive layers. As shown in Fig. 5, the surface morphology of the NI–Cz film vacuum-deposited on the ITO glass substrate was uniform and homogenenerous, and the surface root-mean-square (RMS) roughness was only several nanometers which may be beneficial for improving the device's performance. However, the surface morphology of the NI–TPA film was agglomerative due to the non-planar structure of the triphenylamine moiety. Compared to the NI-Cz film with the coplanar carbazole moiety, the RMS roughness was more than 30 nm which may cause metal penetration during the evaporation process that affected the performance test. We also observed similar morphology on other substrates with different polarities, such as quartz and glass, indicating that it is the interaction between the molecules rather than the interaction between the molecules and the substrate that drives the molecular self-organization. Thus, altering the terminal group in D–A molecules can adjust the film morphology.

3.4. Current–voltage (I–V) characteristics of the memory devices

The electrical switching and memory effects of NI–Cz and NI–TPA were illustrated by *I–V* characteristics of an electronic device with the molecule film sandwiched between the ITO and Al electrodes. Rather than encoding "0" and "1" as the amount of charge stored in a cell in silicon devices, small molecular memory stored date in an entirely different form which was based on the high- and low-conductivity response to an applied voltage. Fig. 6 (a, c) shows the typical *I–V* curves of the small molecular devices fabricated with NI–Cz and NI–TPA. Taking NI–Cz for example, as the initial voltage swept from 0 to −2 V, current is very low and in the order of 10^{-7}–10^{-4} A. It reveals that the device is in a low-conductivity state and assigned as the OFF-state or "0" signal in data storage. However, the continuous sweeping voltage induces an abrupt increase in current around −2.44 V, which is defined as the switching threshold voltage. After switching, the current reaches at almost 3 orders of magnitude higher than that in a low-conductivity state. This increase in current indicates that the device is transformed

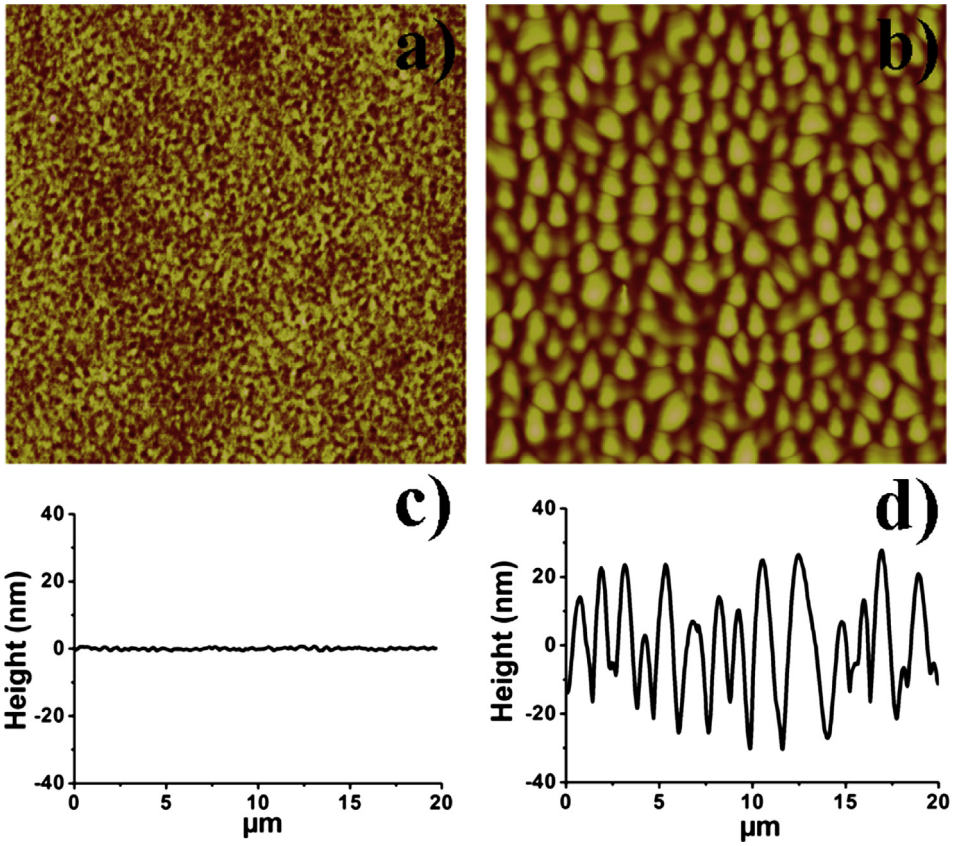

Fig. 5. Tapping-mode (20 μm × 20 μm) AFM topography (a, c); typical cross-section profile of AFM topographic image (b, d) of NI–Cz and NI–TPA films on ITO substrates, respectively.

from the low-conductivity state to a high-conductivity state and assigned as ON-state or "1" signal in data storage. This electronic transition from OFF-state to ON-state serves as the "writing" process. The device remains in a high conductivity (ON-state) during the subsequent second sweep from 0 to −4 V and does not relax to the OFF-state even after the power is turned off for 20 min. As the voltage sweeps negatively from 0 to 4 V, an abrupt decrease in current is observed at a threshold voltage of about 2.88 V, corresponding to the "erasing" process for the memory device. Similarly, the device remains in a low conductivity (OFF-state) during the subsequent fourth sweep from 0 to 4 V and even after the power is turned off. The OFF-state can be further turned on to the ON-state by reapplying the switching threshold voltages, as the fifth sweep shown in Fig. 6a. Therefore, this memory device could be used as a flash type memory. Compared to NI–Cz, the device based on NI–TPA was also a flash type memory, but it showed a much lower turn on threshold voltage of −0.85 V, which revealed by cyclic voltammetry and UV−vis absorption spectroscopy measurement.

The stability of the memory effects was also evaluated under the same atmosphere. Fig. 6 (b, d) showed the retention time tests under a constant stress of 1 V for both the ON and OFF states of the NI–Cz and NI–TPA device, respectively. The ON/OFF current ratios of $10^3 \sim 10^4$ could be maintained and no obvious degradation in current was observed for both the ON and OFF states after periods of at least 10^4 s.

3.5. The probability and stability of the memory devices

Considering the fact that the bistability phenomenon in organic devices is sometimes non-reproducible and unreliable, it is important to investigate the cell-to-cell uniformity for small molecule based devices. Fig. 7 shows the statistical data obtained from 50 cells (10 times for each cell) for the two devices based on either NI–Cz or NI–TPA. For NI–Cz, the turn-on voltage was mainly between −2.2 V and −2.6 V (with yield of 80%), and turn-off voltage was mainly between 2.6 V and 3 V (with yield of 56%). For NI-TPA, the turn-on voltage varied from −0.4 V to −2.0 V, and the turn-off voltage was from 2.4 V to 4.0 V, so it showed no obvious distributed areas. Thus the device based on NI–Cz has better stability and repeatability compared to NI–TPA due to the coplanar carbazole moiety which suggested that the film with the smooth surface was beneficial for improving the probability and stability of high-density data-storage devices.

3.6. Proposed data-storage mechanism

To understand the mechanism for the observed flash-type memory behavior of NI–Cz and NI–TPA system, quantum calculations were carried out at the B3LYP/6-31G(d) level with the Gaussian 03 program package. The carbazole and triphenylamine moieties are well-known as electron donors and 1,8-naphthalimide was also known as electron acceptor. The charge transfer process can occur when the conjugated molecule is activated by electrical stimulation, transferring charges from either the carbazole or triphenylamine to the 1,8-naphthalimide and forming a charge-transfer (CT) state.

It is obvious that the 1,8-naphthalimide moiety contributed more to the LUMO while carbazole/triphenylamine contributed more on the HOMO as shown in Fig. 8. Under an applied field, a hole would be easier to transfer from the Al electrode to NI–Cz (or NI-TPA) memory layer due to the lower hole injection barrier between ITO (–4.8 eV) and HOMO energy which was 0.7 eV than that between Al (– 4.28 eV) and the LUMO energy level was 1.56 eV. With the increase of the bias up to the threshold voltage, more and

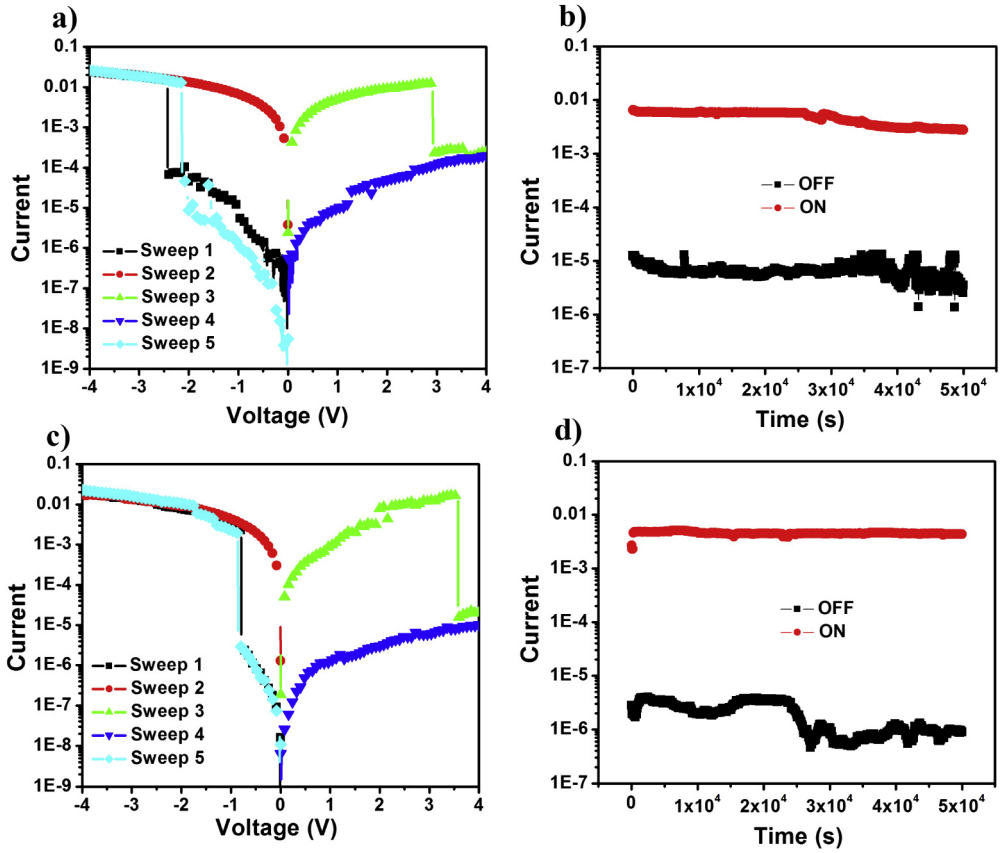

Fig. 6. Current density-voltage (I–V) characteristics and effect of the operation time (at 1 V) on the device current density in the OFF and ON states of the device.

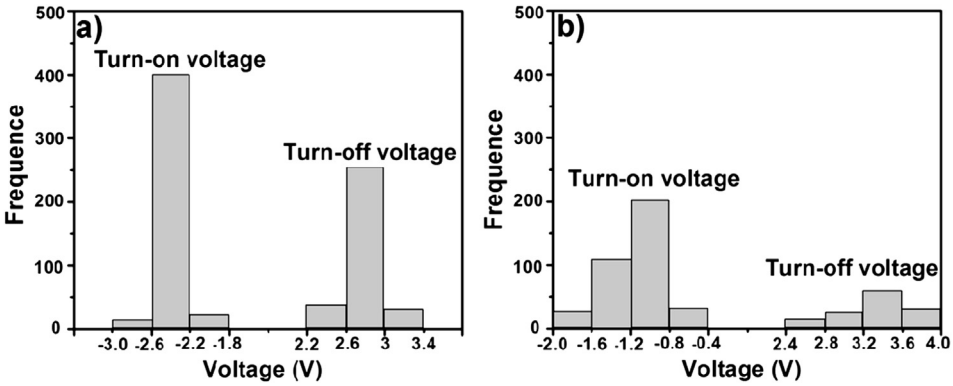

Fig. 7. The statistical data of reproducibility of the devices based NI–Cz (a) or NI–TPA(b).

more charges continue to be generated with high electric field and the positive and negative charges are segregated, leading to the formation of a stable CT complex. Then the device is switched from the OFF state to the ON state. Even after the driving power is turned off, the ON state of the memory device could still remain due to the good stability of the CT complex formed. However, applying an opposite voltage causes the CT complex decomposition and the device returns to the original OFF state. Hence, the memory device based on NI–Cz or NI–TPA exhibits flash memory behavior.

4. Conclusions

In this work, we have successfully synthesized two D—A molecules and demonstrated the effects of the coplanarity of the donor moiety on the reproducibility of switching phenomenon for the memory device, which based on NI–Cz was much better than that based on NI–TPA due to the rigid carbazole moiety in favor of improving the surface morphology, which was revealed by atomic force microscopy measurement. Both devices show flash memory

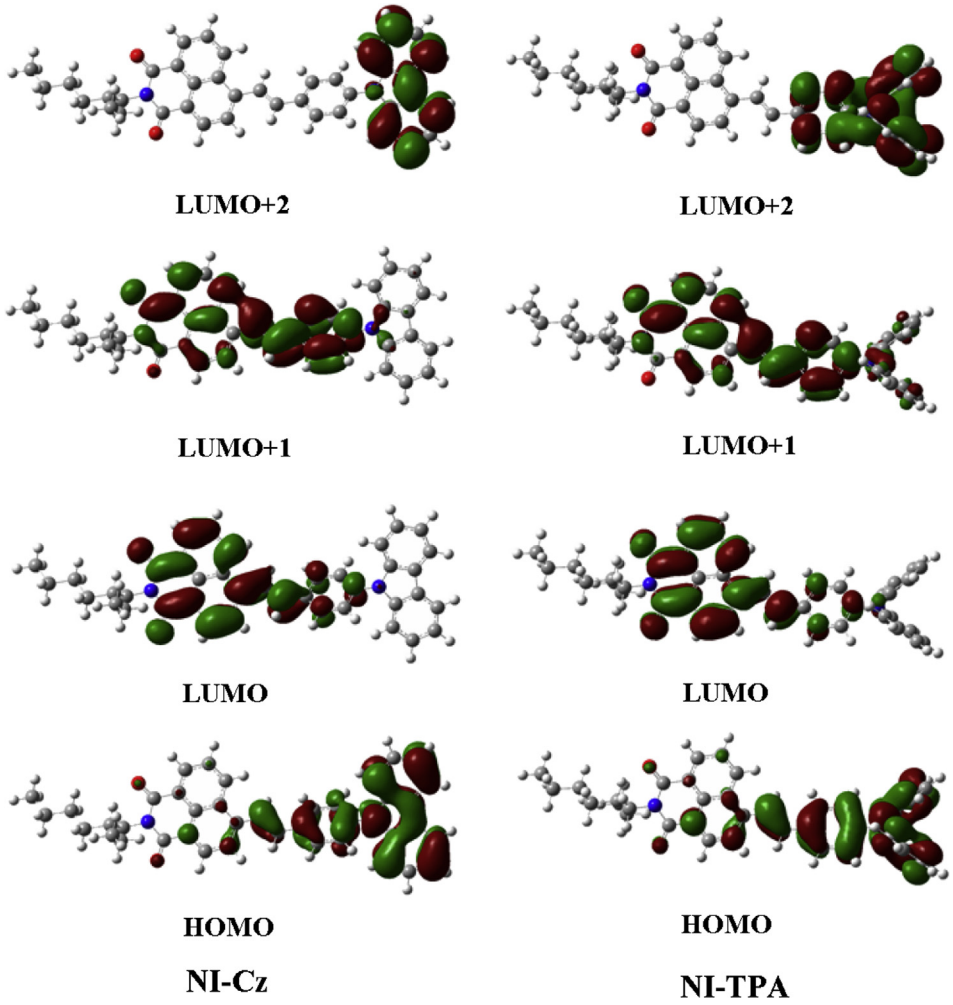

Fig. 8. Optimized geometries and electronic density counters of molecular orbital of NI–Cz and NI–TPA.

behavior due to the formation and dissociation of a charge-transfer complex and their ON/OFF ratios exhibit more than three orders of magnitude at 1 V with a long retention time that is more than 10^4 s. The results provided a new strategy for designing D–A molecules for better reproducibility of switching phenomenon for the memory device.

Acknowledgments

This work was financially supported by the Chinese Natural Science Foundation (21076134, 21176164 and 21206102), NSF of Jiangsu Province (BK2010208), a project of the Department of Education of Jiangsu Province (12KJB430011), Suzhou Nano-project (ZXG2012023) and Project supported by the Specialized Research Fund for the Doctoral Program of Higher Education of China (Grant No. 20113201130003 and 20123201120005). A Project Funded by the Priority Academic Program Development of Jiangsu Higher Education Institutions (PAPD).

References

[1] Lee J, Chang H, Kim S, Bang GS, Lee H. Molecular monolayer nonvolatile memory with tunable molecules. Angewandte Chemie-International Edition 2009;48:8501–4.
[2] Li H, Xu QF, Li NJ, Sun R, Ge JF, Lu JM, et al. A small-molecule-based ternary data-storage device. Journal of the American Chemical Society 2010;132:5542–3.
[3] Chou YH, Lee WY, Chen WC. Self-assembled nanowires of organic n-type semiconductor for nonvolatile transistor memory devices. Advanced Functional Materials 2012;22:4352–9.
[4] Xie LH, Ling QD, Hou XY, Huang W. An effective friedel–crafts post-functionalization of Poly(N-vinylcarbazole) to tune carrier transportation of supramolecular organic semiconductors based on π-stacked polymers for nonvolatile flash memory cell. Journal of the American Chemical Society 2008;130:2120–1.
[5] Ling QD, Chang FC, Song Y, Zhu CX, Liaw DJ, Chan DSH, et al. Synthesis and dynamic random access memory behavior of a functional polyimide. Journal of the American Chemical Society 2006;128:8732–3.
[6] Song S, Cho B, Kim TW, Ji Y, Jo M, Wang G, et al. Three-dimensional integration of organic resistive memory devices. Advanced Materials 2010;22:5048–52.
[7] Park S, Kim K, Kim DM, Kwon W, Choi J, Ree M. High temperature polyimide containing anthracene moiety and its structure, interface, and nonvolatile memory behavior. ACS Applied Materials & Interfaces 2011;3:765–73.
[8] Zhuang XD, Chen Y, Liu G, Li PP, Zhu CX, Kang ET, et al. Conjugated-polymer-functionalized graphene oxide: synthesis and nonvolatile rewritable memory effect. Advanced Materials 2010;22:1–5.
[9] Liu YH, Li NJ, Xia XW, Ge JF, Xu QF, Lu JM. Flash memory effects based on styrene/maleimiade copolymers with pendant azobenzene chromophores. European Polymer Journal 2011;47:1160–7.
[10] You NH, Chueh CC, Liu CL, Ueda M, Chen WC. Synthesis and memory device characteristics of new sulfur donor containing polyimides. Macromolecules 2009;42:4456–63.
[11] Chou YH, Yen HJ, Tsai CL, Lee WY, Liou GS, Chen WC. Nonvolatile transistor memory devices using high dielectric constant polyimide electrets. Journal of Materials Chemistry C 2013;1:3235–43.
[12] Liu SJ, Lin WP, Yi MD, Xu WJ, Tang C, Zhao Q, et al. Conjugated polymers with cationic iridium(III) complexes in the side-chain for flash memory devices utilizing switchable through-space charge transfer. Journal of Materials Chemistry 2012;22:22964–70.
[13] Yin CR, Han Y, Li L, Ye SH, Mao WW, Yi MD, et al. Hindrance-functionalized π-stacked polymer based on polystyrene with pendent cardo groups for organic electronics. Polymer Chemistry 2013;4:2540–5.
[14] Kim J, Cho S, Choi S, Baek S, Lee D, Kim O, et al. Novel electrical properties of nanoscale thin films of a semiconducting polymer: quantitative current-sensing AFM analysis. Langmuir 2007;23:9024–30.
[15] Lee TJ, Chang CW, Hahm SGu, Kim K, Park S, Kim DM, et al. Programmable digital memory devices based on nanoscale thin films of a thermally dimensionally stable polyimide. Nanotechnology 2009;20:135204–20.
[16] Fan NY, Liu HF, Zhou QH, Zhuang H, Li Y, Li H, et al. Memory devices based on functionalized copolymers exhibiting a linear dependence of switch threshold voltage with the pendant nitro-azobenzene moiety content change. Journal of Materials Chemistry 2012;22:19957–63.
[17] Hahm SG, Choi S, Hong SH, Lee TJ, Park S, Kim DM, et al. Novel rewritable, non-volatile memory devices based on thermally and dimensionally stable polyimide thin films. Advanced Functional Materials 2008;18:3276–82.
[18] Baker CO, Shedd BO, Tseng ROJ, Morales AAM, Ozkan CS, Ozkan M, et al. Size control of gold nanoparticles grown on polyaniline nanofibers for bistable memory devices. ACS Nano 2011;5:3469–74.
[19] Lai PY, Chen JS. Electrical bistability and charge transport behavior in Au nanoparticle/poly(N-vinylcarbazole)hybrid memory devices. Applied Physics Letters 2008;93:153305–7.
[20] Li FS, Son DI, Seo SM, Cha HM, Kim HJ, Kim BJ, et al. Organic bistable devices based on core/shell CdSe/ZnS nanoparticles embedded in a conducting poly(N-vinylcarbazole) polymer layer. Applied Physics Letters 2007;91:122111–3.
[21] Miao SF, Li H, Xu QF, Li YY, Ji SJ, Li NJ, et al. Tailoring of molecular planarity to reduce charge injection barrier for high-performance small-molecule-based ternary memory device with low threshold voltage. Advanced Materials 2012;24:6210–5.
[22] Miao SF, Li H, Xu QF, Li NJ, Zheng JW, Sun R, et al. Molecular length adjustment for organic azo-based nonvolatile ternary memory devices. Journal of Materials Chemistry 2012;22:16582–9.
[23] Zhang YH, Zhuang H, Yang Y, Xu XF, Bao Q, Li NJ, et al. Thermally stable ternary data-storage device based on twisted anthraquinone molecular design thermally stable ternary data-storage device based on twisted anthraquinone molecular design. The Journal of Physical Chemistry C 2012;116:22832–9.
[24] Ren WS, Zhu YX, Ge JF, Xu XF, Sun R, Li NJ, et al. Bistable memory devices with lower threshold voltage by extending the molecular alkyl-chain length. Physical Chemistry Chemical Physics 2013;15:9212–8.
[25] Zhuang H, Zhang QJ, Zhu YX, Xu XF, Liu HF, Li NJ, et al. Effects of terminal electron acceptor strength on film morphology and ternary memory performance of triphenylamine donor based devices. Journal of Materials Chemistry C 2013;1:3816–24.
[26] Chou YH, You NH, Kurosawa T, Lee WY, Higashihara T, Ueda M, et al. Thiophene and selenophene donor–acceptor polyimides as polymer electrets for nonvolatile transistor memory devices. Macromolecules 2012;45:6946–56.
[27] Lee WY, Kurosawa T, Lin ST, Higashihara T, Ueda M, Chen WC. New donor–acceptor oligoimides for high-performance nonvolatile memory devices. Chemistry of Materials 2011;23:4487–97.
[28] Liu CL, Kurosawa T, Yu AD, Higashihara T, Ueda M, Chen WC. New dibenzothiophene-containing donor–acceptor polyimides for high-performance memory device applications. The Journal of Physical Chemistry C 2011;115:5930–9.
[29] Wang P, Liu SJ, Lin ZH, Dong XC, Zhao Q, Lin WP, et al. Design and synthesis of conjugated polymers containing Pt(II) complexes in the side-chain and their application in polymer memory devices. Journal of Materials Chemistry 2012;22:9576–83.
[30] Li H, Jin ZN, Li NJ, Xu QF, Gu HW, Lu JM, et al. A small-molecule-based device for data storage and electro-optical switch applications. Journal of Materials Chemistry 2011;21:5860–2.
[31] Gudeika D, Michaleviciute A, Grazulevicius JV, Lygaitis R, Grigalevicius S, Jankauskas V, et al. Structure properties relationship of donor-acceptor derivatives of triphenylamine and 1,8-Naphthalimide. The Journal of Physical Chemistry C 2012;116:14811–9.
[32] Aljarilla A, Arroyo LL, Cruz PDL, Oswald F, Meyer TB, Langa F. Organic dyes incorporating oligothienylenevinylene for efficient dye-sensitized solar cells. Organic Letters 2012;14:5732–5.
[33] Cai N, Wang YL, Xu MF, Fan Y, Li RZ, Zhang M, et al. Engineering of push–pull thiophene dyes to enhance light absorption and modulate charge recombination in mesoscopic solar cells. Advanced Functional Materials 2013;23:1846–54.
[34] Wang ZH, Liang M, Wang LN, Hao YJ, Wang C, Sun Z, et al. New triphenylamine organic dyes containing dithieno[3,2-b:2′,3′-d]pyrrole (DTP) units for iodine-free dye-sensitized solar cells. Chemical Communications 2013;49:5748–50.
[35] Cheng XB, Sun SY, Liang M, Shi YB, Sun Z, Xue S. Organic dyes incorporating the cyclopentadithiophene moiety for efficient dye-sensitized solar cells. Dyes and Pigments 2012;92:1292–9.
[36] Wan ZQ, Jia CY, Zhou LL, Huo WR, Yao XJ, Shi Y. Influence of different arylamine electron donors in organic sensitizers for dye-sensitized solar cells. Dyes and Pigments 2012;95:41–6.
[37] Etzold F, Howard IA, Mauer R, Meister M, Kim TD, Lee KS, et al. Ultrafast exciton dissociation followed by nongeminate charge recombination in PCDTBT: PCBM photovoltaic blends. Journal of the American Chemical Society 2011;133:9469–79.
[38] Zhang B, Chen YJ, Zhang YF, Chen XD, Chi ZG, Yang J, et al. The steric effect of aromatic pendant groups and electrical bistability in π-stacked polymers for memory devices. Physical Chemistry Chemical Physics 2012;14:4640–50.
[39] Cowan SR, Banerji N, Leong WL, Heeger AJ. Charge formation, recombination, and sweep-out dynamics in organic solar cells. Advanced Functional Materials 2012;22:1116–28.